P13A.13 USING A LOW-ORDER MODEL TO DETECT AND CHARACTERIZE TORNADOES IN MULTIPLE-DOPPLER RADAR DATA

Corey K. Potvin*[,1], Alan Shapiro[1], Tian-You Yu[2], Jidong Gao[3] and Ming Xue[1,3]
[1]School of Meteorology, University of Oklahoma, Norman, OK
[2]School of Electrical and Computer Engineering, University of Oklahoma, Norman, OK
[3]Center for Analysis and Prediction of Storms, Norman, OK

1. INTRODUCTION

Several methods have been used to fit low-order models of velocity fields to radial velocity data from a single Doppler radar. The Velocity-Azimuth Display (VAD; Lhermite and Atlas 1962) and Volume Velocity Processing (VVP; Waldteufel and Corbin 1979) techniques use spatially-linear wind models, and are often successful as long as the conditions for their validity are approximately met. A relatively new class of low-order wind models is being used to analyze hurricanes and tornadoes: the Velocity Track Display (VTD, Lee et al. 1994), Extended Velocity Track Display (EVTD; Roux and Marks 1996) and the Ground-Based Velocity Track Display (GBVTD, Lee at al. 1999, Lee and Marks 2000). These methods seek to obtain the key axisymmetric and low-order asymmetric components of the tangential wind from a harmonic analysis of radial velocity data from a single Doppler radar.

Dual-Doppler techniques have been developed to take advantage of the additional information gained by sampling a wind field from multiple radar perspectives (Shapiro and Mewes 1999; Gao et al. 1999). These techniques often use mass conservation as a strong or weak constraint. Dual-Doppler analysis has proven to be an extremely useful tool in examining the evolution of 3-D wind fields and derived quantities (e.g. terms in vorticity budget) within tornadic supercell thunderstorms (Ray et al. 1981, Brandes 1981, Brandes 1984). The GBVTD technique has recently been extended to two radars, thereby allowing a portion of the vortex-relative radial wind component to be recovered, and improving the accuracy of the retrieved tangential wind (Liou et al. 2006).

This study describes a new multiple-Doppler radar analysis technique for the objective detection and characterization of tornadoes. Radial wind data are fit to an analytical low-order model of a tornado and its near environment in order to retrieve key characteristics of the wind field, particularly the location, size and strength of the tornado. Observations are used at the locations and times they are acquired, thus bypassing the need for interpolation, moving reference frames or other ad hoc procedures. The method requires that multiple first guesses for the vortex center location be used in order to maximize the probability of detection.

The technique is being designed for use in CASA (Collaborative Adaptive Sensing of the Atmosphere; McLaughlin et al. 2005) networks of densely-spaced, adaptively scanning radars. It exhibits skill in retrieving important characteristics of tornado-like circulations in a simulated CASA-like domain.

2. LOW-ORDER MODEL

The tornado model is a combination of four idealized flow fields: a uniform flow,

* *Corresponding Author Address:* Corey Potvin, Univ. of Oklahoma, School of Meteorology, Norman, OK 73019; email: corey.potvin@ou.edu

linear shear flow, linear divergence flow, and modified combined Rankine vortex (representing the tornado). The latter three fields are allowed to translate. The model consists of 17 parameters, including vortex center, translation and radius, as well as maxima and decay rates of the tangential and radial wind components (Table 1). Model winds are projected in the direction of the radar(s) to obtain the model radial wind, V_r:

$$
\left.
\begin{aligned}
V_r = {} & \frac{(x_n - x)}{r_n}\left[a + b(y - vt) + c(x - ut) + \frac{V_R}{R}(x - x_0 - u_v t) - \frac{V_T}{R}(y - y_0 - v_v t)\right] + \\
& \frac{(y_n - y)}{r_n}\left[d + e(x - ut) + f(y - vt) + \frac{V_R}{R}(y - y_0 - v_v t) - \frac{V_T}{R}(x - x_0 - u_v t)\right] \qquad r < R, \\
= {} & \frac{(x_n - x)}{r_n}\left[a + b(y - vt) + c(x - ut) + \frac{R^\beta V_R (x - x_0 - u_v t)}{r^{\beta+1}} - \frac{R^\alpha V_T (y - y_0 - v_v t)}{r^{\alpha+1}}\right] + \\
& \frac{(y_n - y)}{r_n}\left[d + e(x - ut) + f(y - vt) + \frac{R^\beta V_R (y - y_0 - v_v t)}{r^{\beta+1}} - \frac{R^\alpha V_T (x - x_0 - u_v t)}{r^{\alpha+1}}\right] \qquad r \geq R.
\end{aligned}
\right\}
$$

where (x_n, y_n) are the radar locations,

$r_n = \sqrt{(x_n - x)^2 + (y_n - y)^2}$ and

$r = \sqrt{(x - x_0 - u_v t)^2 + (y - y_0 - v_v t)^2}$.

Table 1. Parameters in low-order model.

Parameter	Description
a,d	uniform flow
b,e	shear field strength
c,f	divergence field strength
u,v	shear/divergence field translation
x_0,y_0	modified Rankine-combined vortex center
R	vortex radius of maximum wind
V_T,V_R	maximum tangential, radial winds
u_v,v_v	vortex translation
α,β	tangential, radial wind decay exponents

3. COST FUNCTION COMPUTATION AND OPTIMIZATION

The (squared) discrepancies between the observed and model-predicted wind fields are summed over the spatial-temporal domains of *N* radars, each scanning in range *R*, azimuth θ and elevation angle Φ. Discrepancy calculations are performed at the same locations and times as the wind observations, so no spatial or temporal interpolation procedures are required. The use of observational data at the actual locations and times they are obtained is a strength of our methodology.

Radar resolution volumes increase in size with distance from the radar, and thus their associated wind observations become representative of data over a larger region as range increases. A range-weighting factor, r_n/r_{mean} , is introduced to account for this. In reality, radar resolution volumes increase as the square of range, but in our

experiments, resolution volumes are considered to be flat due to the "cylindrical" radar geometry. However, it has been verified that the results are very similar regardless of which of these weighting functions is used.

The cost function accounting for the discrepancies between observed and model winds is

$$J = \sum_{n=1}^{N} \sum_{m=1}^{M} \sum_{\phi} \sum_{\theta} \sum_{R} \left[\frac{\text{Range}}{\text{Range}_{\text{mean}}} \left(V_r^{\text{obs}} - V_r^{\text{mod}} \right)^2 \right]$$

where *M* is the total number of full volume scans (temporal sum). J is minimized in order to retrieve the set of parameter values producing the least squares error in the model wind (the best fit between the model and observed winds). Due to the nonlinearity of our problem, a conjugate gradient method is used. In this type of method, a vector of provisional values for the model parameters is systematically updated by the algorithm such that the minimum in J is iteratively approached.

As with other minimization techniques, multiple minima in J can prevent the global minimum from being retrieved. Local minima in our case can result from the intrinsic non-linearity of the problem, as well as from areas of missing data and departure of the observed wind field from the model.

The threat of local minima increases as the surface of the cost function becomes more elliptical, since even small errors may be sufficient to produce spurious minima. In order to reduce the ellipticity of J, the first guess vector is scaled such that the gradients of J with respect to each of the parameters become closer in magnitude. To accomplish this, the scaling factors are set equal to physically realistic values of each of the parameters. Experiments have shown the technique to be relatively insensitive to the selection of scaling factors for physically reasonable ranges of these factors.

4. EXPERIMENTS

The low-order technique is tested using (i) analytically-generated vortices and surrounding broadscale flow and (ii) ARPS-simulated (Advanced Regional Prediction System; Xue et al. 2001) wind observations of a tornado and its near-environment (Figure 1). Observations in the analytical experiments are calculated from the low-order model, and thus represent an overly-optimistic (identical twin) framework. However, significant random errors (described below) were added to the analytical radial wind data in order to partially mitigate this problem. Both the idealized nature of the input wind field and the ability to specify the true wind parameter values facilitated testing of the algorithm code and identification of potential problems inherent to the technique. In contrast, the ARPS-simulated tornado is not constrained by the low-order model and therefore poses a greater challenge to the technique. Data in the ARPS experiments are trilinearly-interpolated from the ARPS grid to the radar domain. Since the radar domain is generally coarser than the ARPS domain, the radial wind field sampled by the algorithm loses some of the finer features in the ARPS wind field, particularly at larger ranges from the radar.

To simulate weighted averaging of actual radar moment data within a resolution volume, simple range- and beam-weighting functions are applied to a distribution of hypothetical scatterers within each resolution volume in both experiment types. In most of the analytical experiments, Gaussian random errors are added to the volume-averaged observations, with the first standard

deviation of the percent error distribution typically lying between -30 % and 30 %, and the portions of the distribution beyond +/- 50 % being truncated at +/- 50 %. These input errors are large in magnitude and represent serious contamination of the otherwise "optimistic" test data. No error is added to V_r observations in the ARPS experiments.

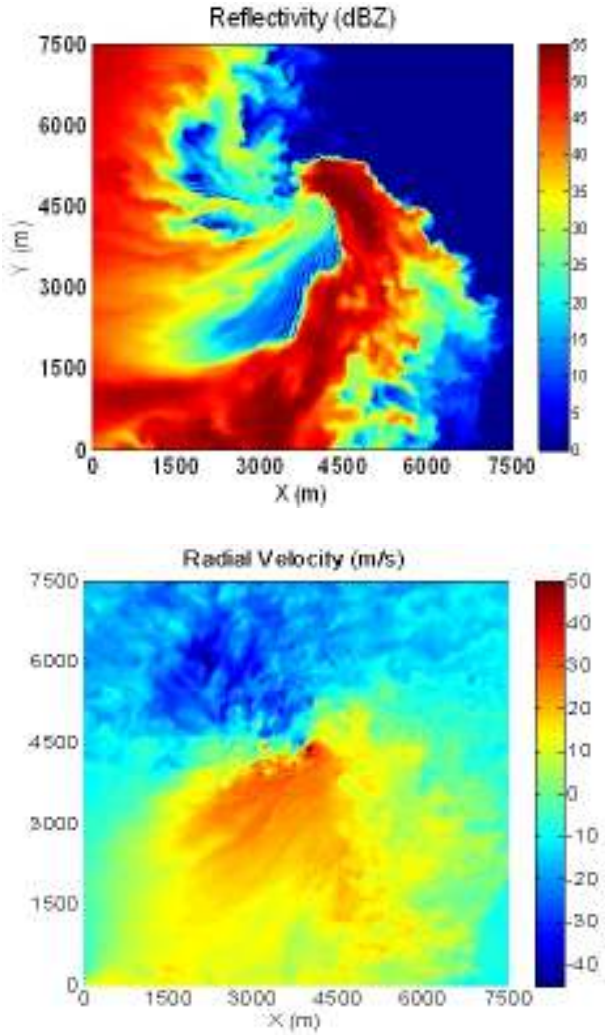

Fig. 1. Reflectivity (top) and radial wind (bottom) fields from the ARPS dataset used in experiments. The emulated radar is located at (0, 0).

The radar-vortex configuration used in our simulation experiments is depicted in Figure 2. Only observations taken within a circular 2 km radius sub-region centered on the first guess for the vortex center are used. Radars are positioned to give a cross-beam angle of ~ 90°. In experiments with the ARPS simulation, the tornado is located roughly 28 km from both radars, which are separated by 40 km (representative of a CASA domain). A radar-tornado distance of ~7 km was used in the analytical experiments described below. In the ARPS experiments, wind data are simultaneously valid over the spatial domain at each model time step and so radar sector scans are assumed instantaneous. A return period of 30 s between three consecutive radar scans is used, giving a temporal domain of 60 s. In all experiments presented below, the radars sampled at 100 m range intervals, every 0.5° or 1.0° in azimuth, and over a single elevation angle of 0.5°. A beamwidth of 2.0° was chosen to approximate that of current experimental CASA radars.

First guess errors were typically set to +50 % of the true parameter value in the analytical experiments, except errors in the vortex center normally ranged over ~1-2 km. In the experiments with ARPS data, the first guess for most parameters was set to zero, except for R (=100 m), α (=0.7), β (=0.7), and x_0 and y_0 (varied according to initial time of retrieval).

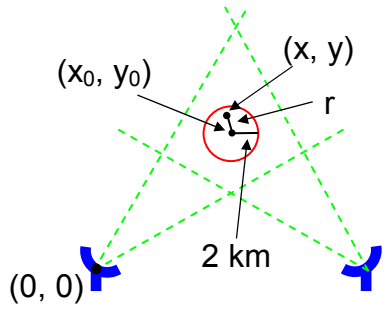

Fig. 2. Radar-vortex geometry and analysis domain.

5. RESULTS

a. Parameter aliasing

Preliminary experiments with analytically-generated data revealed that retrieval of the shear and divergence field translation parameters (u, v) is an ill-posed problem (non-uniqueness). Figure 3 shows a 2-D cross-section of J(u, v) for the case where the remaining model parameters are set equal to truth and no error is added to the radial wind observations. The global minimum in J, corresponding to the correct solution (u, v) = (10, 10) ms^{-1}, is seen to be embedded within a very flat region of J(u, v). Similar results were obtained using the ARPS-simulated wind field. Due to the existence of these flat regions in J, any departure of the wind field from the model can potentially create local minima that may be even lower in value than J is at the correct solution. Thus, a large number of potential solutions for (u, v) exists in practice. The low-order model was therefore modified such that the translation of the vortex and the broadscale wind fields are controlled by a single pair of parameters rather than a separate set for the vortex and for the broadscale. Fortunately, the inability to accurately retrieve the broadscale translation has little negative impact on the retrieval of the remaining vortex and broadscale parameters, both in the analytical and in the ARPS experiments.

Similar but much less significant aliasing also occurs between the shear and divergence parameters. The resulting errors, particularly in the vortex parameters, are very small. Aliasing also occurs between R, V_T, V_R, α, and β due to the finite spacing between observations and, in the ARPS experiments, due to non-linearities in the sampled wind field (in particular, the existence of vortex-like circulations on multiple scales).

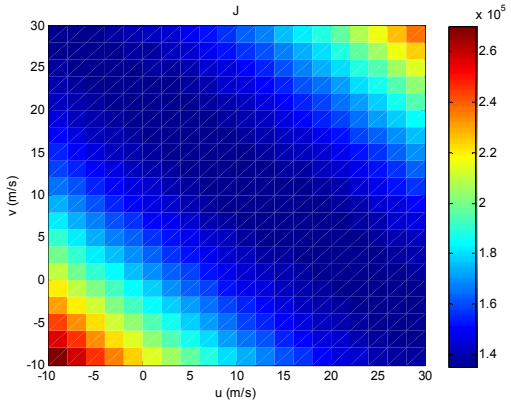

Fig. 3. J(u, v) with perfect first guess for remaining parameters.

Objective detection criteria will need to account for aliasing between vortex parameters by evaluating the retrieved vortex field as a whole rather than treating parameters as independent from each other.

b. First Guess Vortex Center

In order to assess the impact of error in the initialized vortex center, eight retrievals were performed with analytical data using a circular analysis domain of 2 km radius and vortex center first guesses (FGs) with errors of 1.4 km or 1.84 km. All four retrievals with 1.4 km error converged to a solution very

close to truth. However, retrievals with the maximum error in FG vortex center tended to converge to spurious local minima created by the proximity of the simulated vortex to the edge of the analysis domain. An example of these spurious minima is depicted in the plot of $J(x_0, y_0)$ for the case where the true vortex location is (5000 m, 5000 m), the FG vortex location is (3700 m, 3700 m), and the remaining parameters are set to their first guess values (Figure 4, top panel). The local minima located near the edges of the domain are only slightly larger in value than the global minimum corresponding to the correct solution for (x_0, y_0). The bottom panel of Figure 4 shows $J(x_0, y_0)$ when the remaining model parameters are set equal to the values retrieved in the experiment. During this particular retrieval, the model vortex center converged toward the local minimum present in the lower-left corner of the top plot. Due to the large error in the retrieved vortex center, none of the other vortex parameters were accurately recovered.

Spurious minima in J may be widespread in practice due to missing radar observations, random observational error, and violations of the low-order model in nature, including the presence of non-tornadic vortices or vortex-like circulations. Multiple first guesses for the tornado center should therefore be used in order to maximize the probability of successfully identifying tornadoes when they are present.

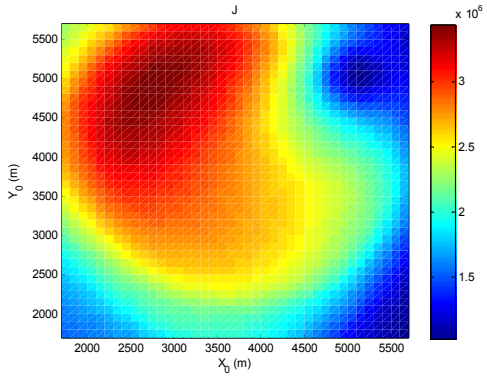

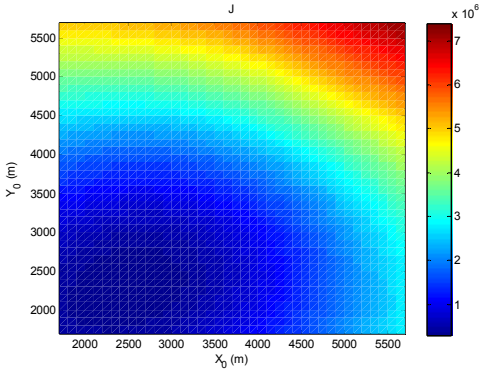

Fig. 4. Plots of $J(x_0, y_0)$ when model parameters set equal to (top) their first guesses and (bottom) their retrieved values.

c. Multiple step approach in ARPS retrievals

Preliminary experiments demonstrated that the tornadic circulation is more reliably retrieved when a multiple-step retrieval procedure is adopted. The procedure used in all experiments presented herein proceeds in two phases. In phase 1, the vortex model parameters are fixed at zero (except for R since this would introduce a "division by zero" computational issue), and the broadscale parameters are retrieved. In phase 2, the radial components of the wind field retrieved in phase 1 is subtracted from the observed radial wind fields, and then the retrieval is repeated on the residual wind field. Since the flow retrieved in phase 1 is much more representative of the broadscale flow than of the tornadic flow, the vortex component of the residual flow is more dominant in the wind field to be retrieved in phase 2. In order to make the retrieval more sensitive to the tornadic flow relative to the (presumably weaker) broadscale flow in phase 2, the cost at each observation point is multiplied by the square of the observed wind:

$$J_{phase2} = \sum_{n=1}^{N}\sum_{m=1}^{M}\sum_{\phi}\sum_{\theta}\sum_{R}\left[(V_r^{obs})^2 \frac{Range}{Range_{mean}}\left(V_r^{obs} - V_r^{mod}\right)^2\right].$$

This multiple step approach was often necessary to the retrieval of the tornado circulation when in close proximity to a non-tornadic, larger-scale vortex-like circulation, such as a mesocyclone. Large circulations may provide a better fit to the model over the whole analysis domain than the smaller-scale tornado vortex. In these cases, a significant portion of the larger vortical circulation is retrieved by the linear broadscale flow parameters in phase 1, thereby increasing the probability that the tornadic circulation will be retrieved in phase 2.

d. Retrievals using ARPS tornado simulation data

Based on results of early retrieval experiments with the ARPS tornado dataset, the emulated radar scanning strategy and the ARPS velocity data were modified in order to present a more realistic test of the technique. Since the sounding velocity had been subtracted from the ARPS simulation in order to maintain the tornado near the center of the domain, the simulated tornado moved very slowly relative to the emulated radars during initial retrieval experiments. This significantly limited the capability of the technique by extending the periods of time over which the tornado could be located between sampled azimuths (and thus be poorly sampled by the radars). In order to increase the rate of change of the two radar-tornado viewing angles, the emulated radars were made to translate at a velocity opposite to that which had been subtracted from the ARPS simulation. The subtracted velocity was then added back onto the ARPS wind data for kinematical consistency. The translation velocity of the observed wind field (including the tornado) relative to the radars' reference frame was thus increased to approximately 20 ms^{-1}.

A series of retrievals was initiated at 30 s intervals over sixteen consecutive 60 s observation periods (~9 min total). An analysis sub-domain radius of 2 km was used in all experiments. Retrieved wind fields were plotted and compared to the corresponding ARPS fields. The retrieved vortex parameter values were examined to determine how well they represented the simulated tornado.

During the ~9 min period over which retrievals were performed, the ARPS-simulated tornado becomes increasingly intense and distinct from the surrounding flow. For much of the beginning of the test period, a non-tornadic circulation is located east of the tornado vortex within the analysis sub-domain. The first guess for the vortex center was placed ~500 m east of the actual tornado for the first set of tests discussed herein; the first guess error was increased to ~1000 m in the second set of tests, during which time the tornado was better defined and thus more amenable to retrieval. Using the larger first guess error in the first set of experiments produced very poor retrievals due to the weakness of the simulated tornado. Unfortunately, the algorithm tended to retrieve the secondary vortex rather than the actual tornado (Figure 5), even when sampling interval and beamwidth were decreased to 0.5° and 1.0°, respectively. However, in all cases, the tornado was successfully retrieved using a nearly perfect first guess for the vortex center, despite the presence of the non-tornadic circulation and of a broader, stronger circulation within the analysis subdomain. This highlights the need to use multiple first guesses for the vortex center in order to increase the probability of detecting weak tornadoes.

By t=200 s in the ARPS simulation, the simulated tornado has become sufficiently distinct from the surrounding flow to be detected by the algorithm despite large

error in the first guess vortex center. Figure 6 illustrates the operation of the two-step retrieval procedure for this case. Subtraction of the retrieved broadscale flow from the ARPS wind field removed a significant portion of the larger scale circulation present at this time. The retrieved vortex is roughly collocated with and somewhat larger than the ARPS tornado. The emulated radar data which were input to the algorithm at this time are shown in figure 7. The algorithm is thus able to detect the simulated tornado and provide useful estimates of its location, size and intensity even though it is too weak to be visually discerned in emulated radar moment data.

In some cases, the retrieved vortex contained significant portions of both the tornado and the immediately adjacent flow (see Figure 8). This resulted from the inability of the low-order model to retrieve and subtract the non-linear non-tornadic flow in phase 1. The retrieved maximum tangential wind occasionally significantly underestimated that of the simulated tornado (Figure 9), an effect which, along with overestimation of vortex radius, results in part due to limited observational resolution, which acts to smear finer-scale features. However, these biases also occur when the observed wind field violates the low-order model in such a way that portions of the larger-scale flow are recovered by the vortex parameters, as in the case already presented in Figure 8.

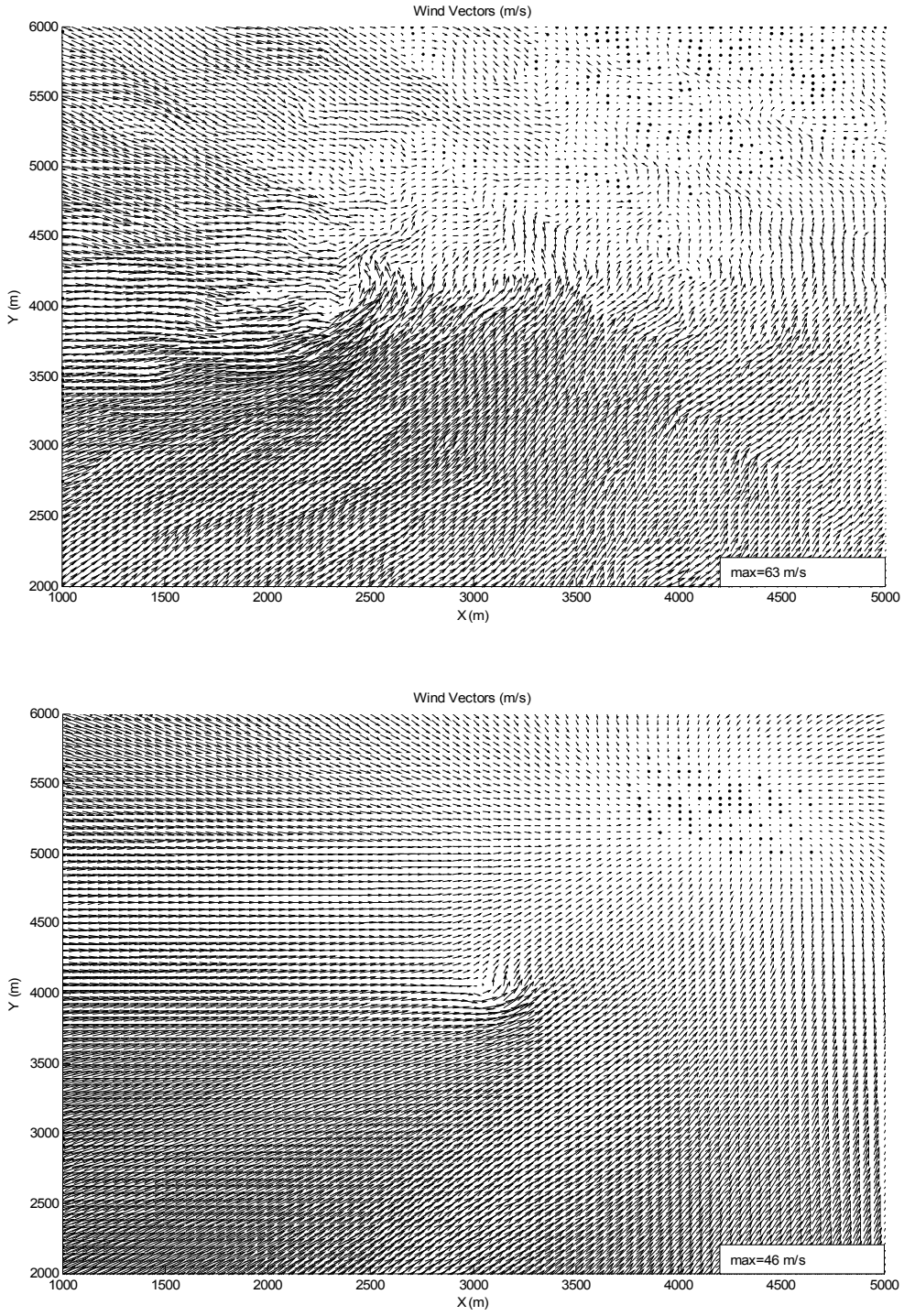

Fig. 5. ARPS (top) and retrieved (bottom) wind fields at t=50s. Every other vector omitted for readability. Plot domain circumscribes the circular analysis sub-domain used in the retrieval.

(a)

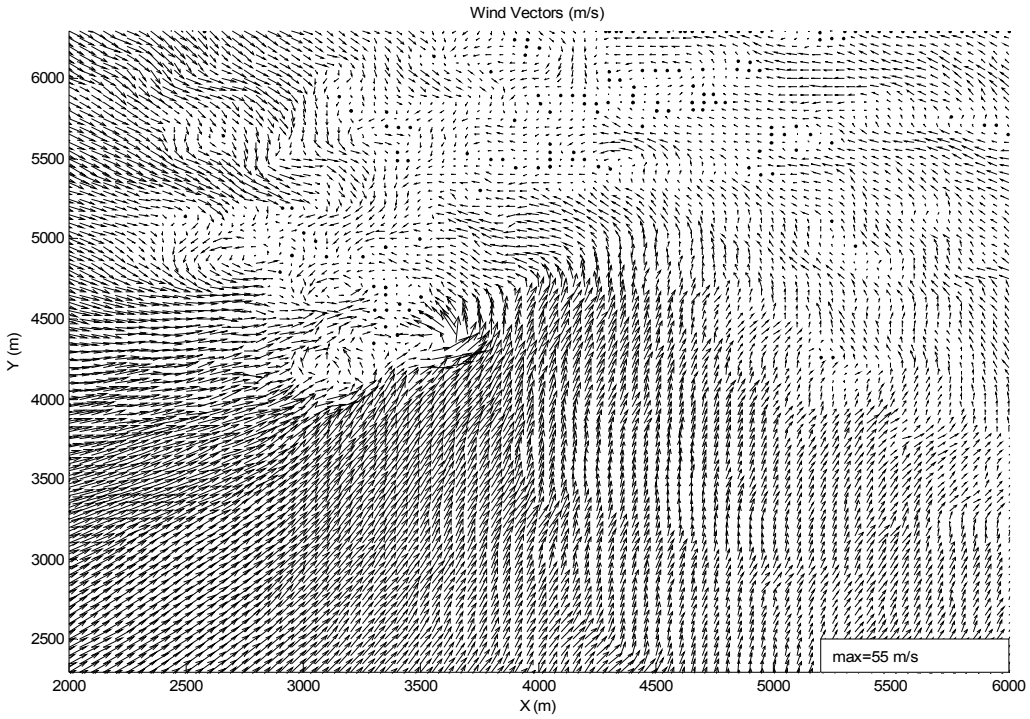
Wind Vectors (m/s)
Y (m)
X (m)
max=55 m/s
2000
2500
3000
3500
4000
4500
5000
5500
6000

(b)

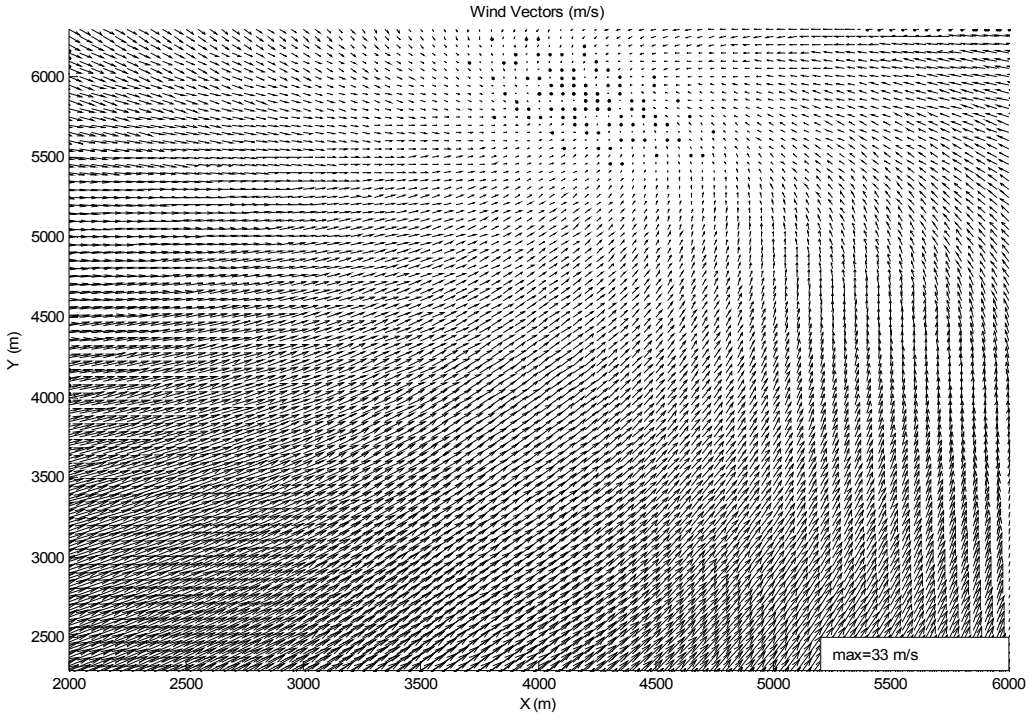
Wind Vectors (m/s)
Y (m)
X (m)
max=33 m/s
2000
2500
3000
3500
4000
4500
5000
5500
6000

(c)

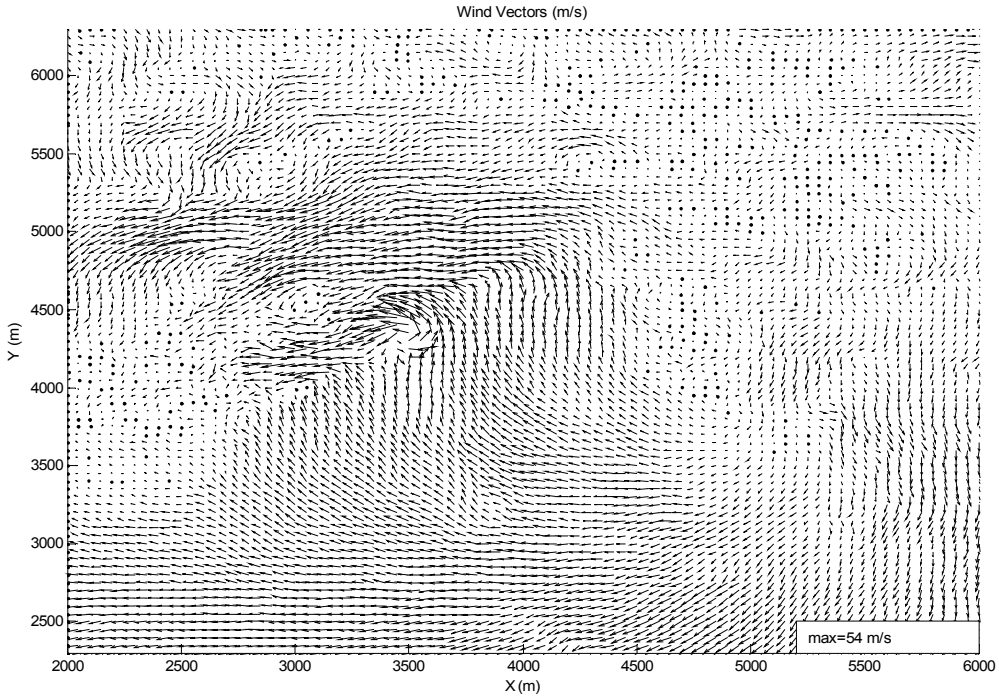

(d)

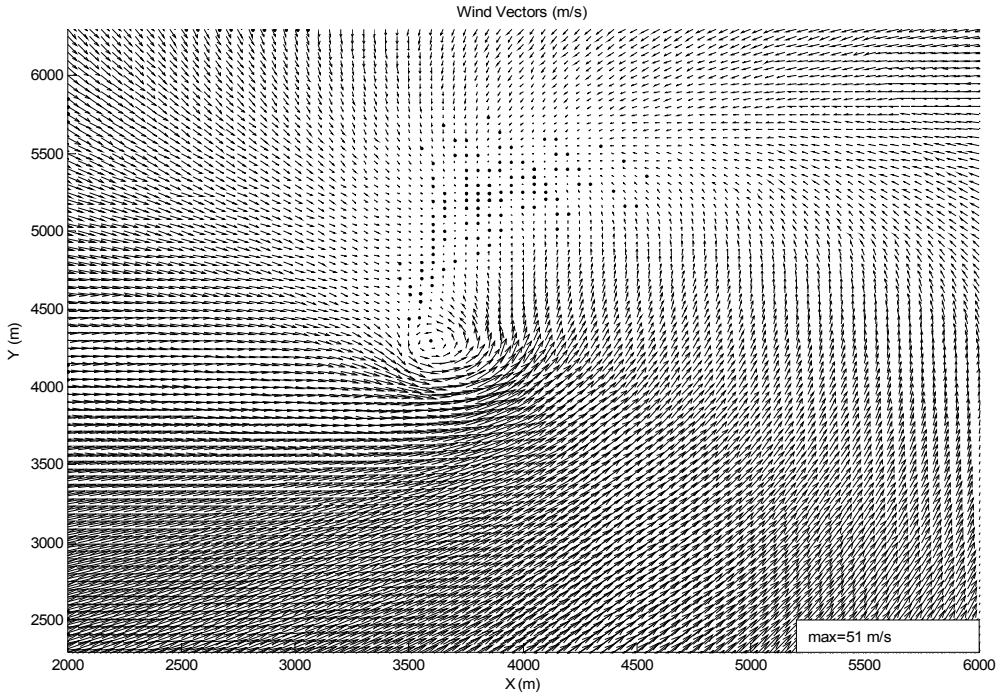

Fig. 6. Illustration of multiple-step retrieval procedure, valid at t=200s: (a) ARPS wind field, (b) retrieved broadscale flow, (c) the vector difference (a)-(b), and (d) total retrieved flow.

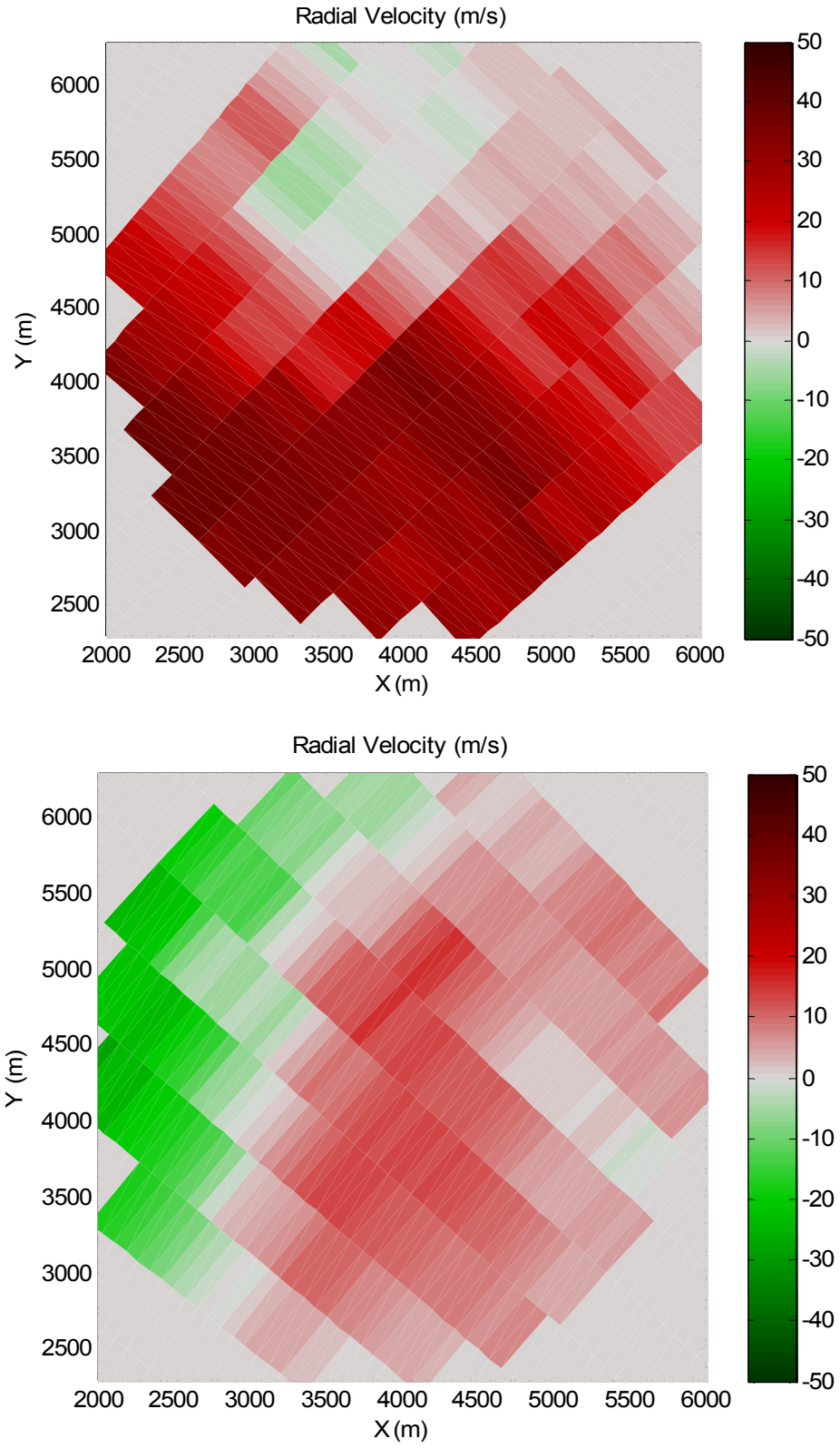

Fig. 7. Emulated radial velocity observations input to retrieval algorithm at t=200s. (top) Vr from radar at x = -15 km, y= -15 km; (bottom) Vr from radar at x = 25 km, y= -15 km.

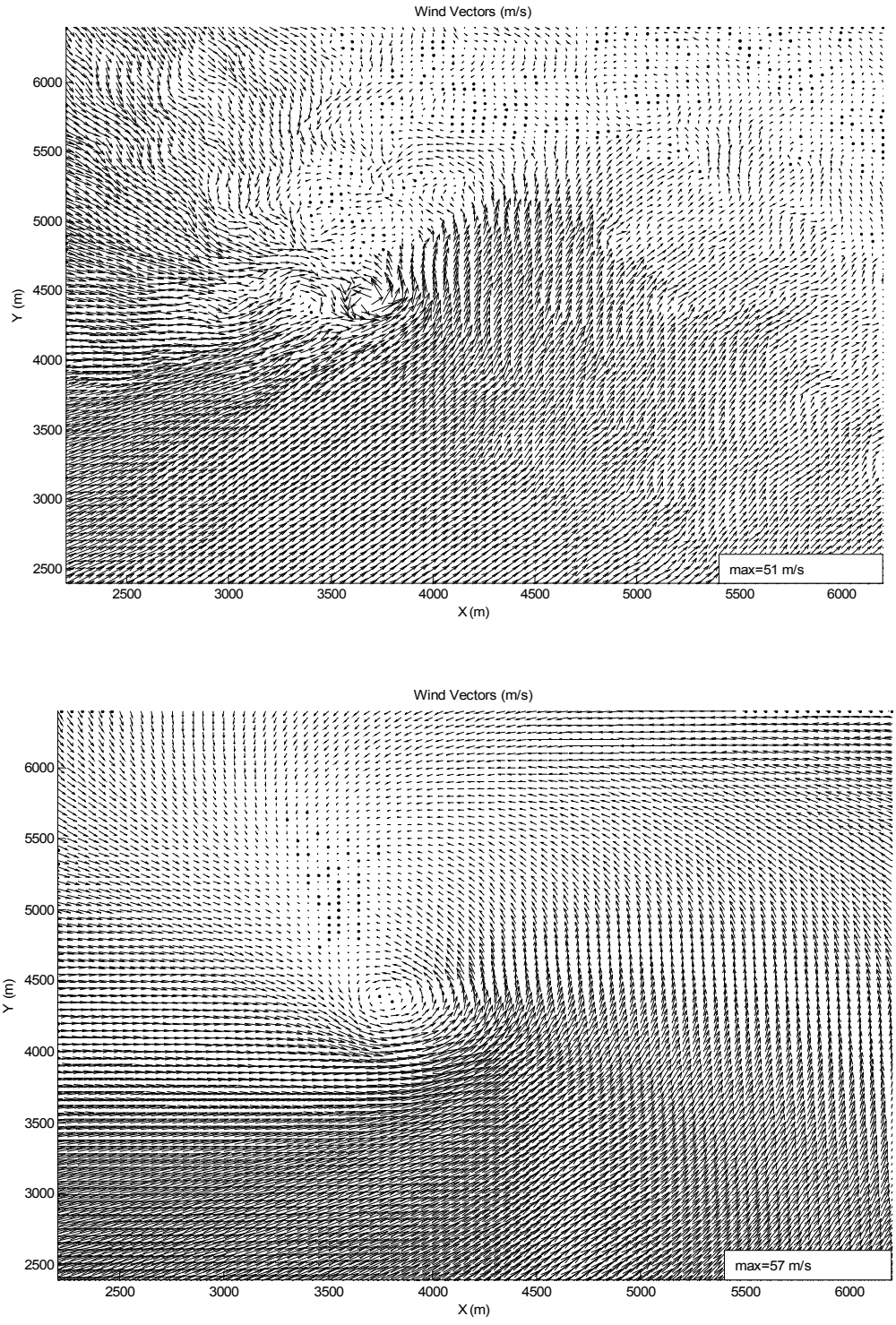

Fig. 8. As in Fig. 5 but for t=260s.

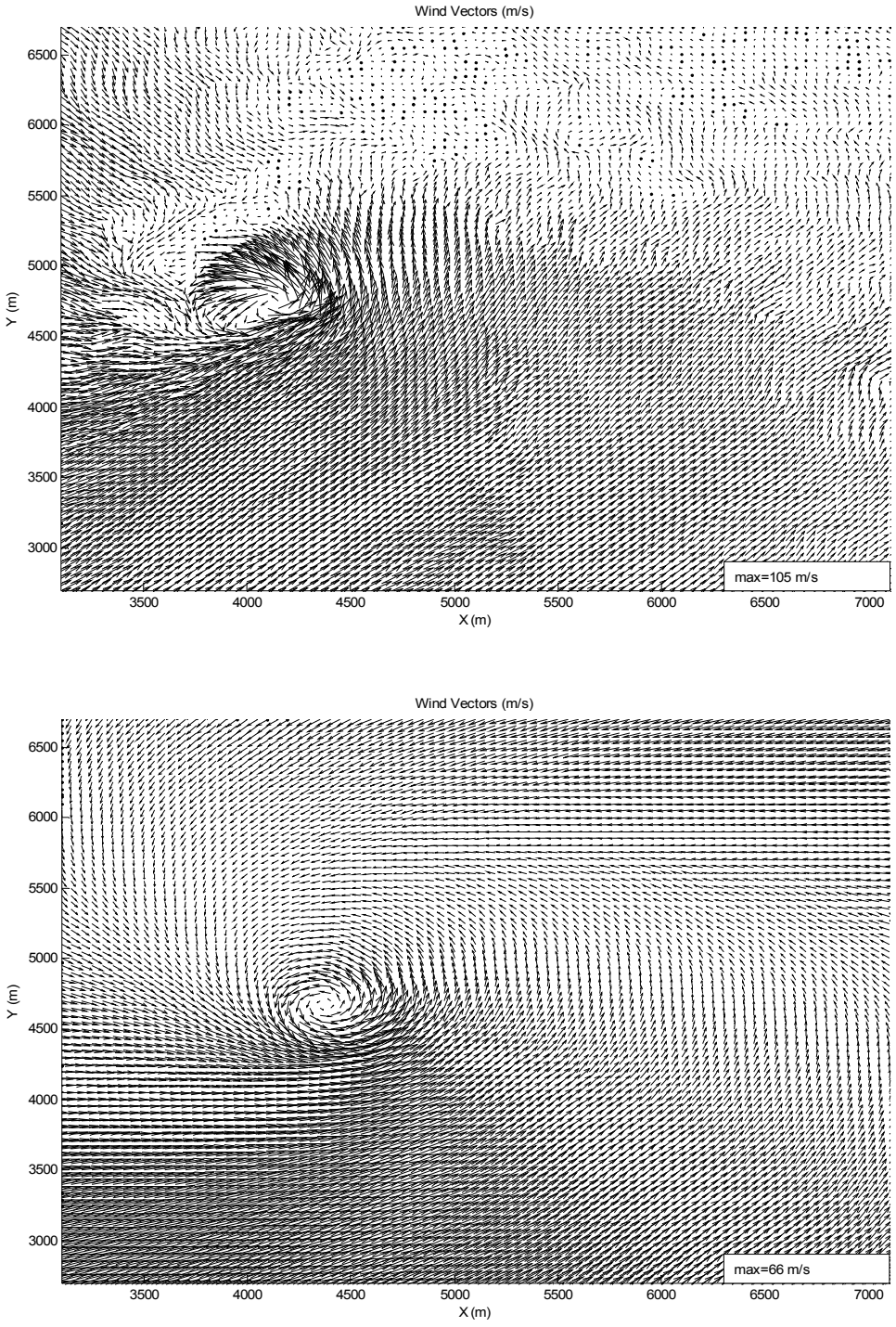

Fig. 9. As in Fig. 5 but for t=440s.

The retrieved vortex and ARPS-estimated tornado paths over the temporal domain of the retrieval experiments (7.5 mins) are compared in Figure 10. The latter path corresponds to the minimum in the ARPS pressure field near the height where observations were taken. This pressure minimum is assumed to correspond to the tornado center. The large rightward bias during the first half of the retrieval period has already been attributed to retrieval of a non-tornadic vortex-like circulation which existed east of the tornado when the tornado was weak. Since this problem is easily resolved by using multiple first guesses for the vortex center (some of which would exclude the second circulation from the analysis subdomain), evaluation of the retrieved vortex path during the second half of the period is more critical to our purpose. Between 290 s and 500 s, the estimated mean and maximum errors in retrieved vortex center were 156 m and 270 m, respectively, indicating that the method is skillful in identifying the location of a detected tornado.

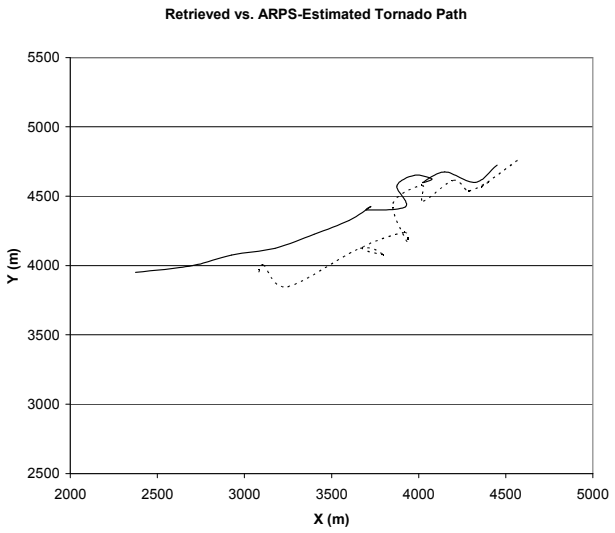

Fig. 10. ARPS-estimated tornado path (solid) and retrieved vortex path (dotted) over retrieval period.

6. CONCLUSIONS

A new multiple-Doppler technique for identifying and characterizing tornadoes and their near-environment has been presented. The method takes advantage of the enhanced density (and therefore spatial coverage and resolution) of a CASA-like radar network. The retrieval technique has been tested against both analytically-generated observations and a high-resolution ARPS simulation of a tornado and surrounding wind field. The technique exhibits skill not only in detecting tornadoes within a CASA domain, but also in retrieving important tornado characteristics including location, size, and strength.

Spurious minima can pose a serious threat to the minimization algorithm's ability to converge to the correct minimum, especially when the first guess wind field (particularly the location of the vortex center) deviates significantly from the observed field. Boundary minima in $J(x_0, y_0)$ can occur near the edge of the analysis domain, and local minima can occur in other multi-dimensional cross-sections of J due to observational error or deviations of the observed wind field from the low-order model. This local minima problem necessitates the use of multiple first guesses for the location of the vortex and of a two-step approach in which much of the larger-scale flow is retrieved and subtracted before the vortex retrieval is performed. The latter strategy is necessary in cases where a non-tornadic vortex-like circulation provides a better fit to the low-order model than the tornado itself. Another possible solution which will be tested is to revise the low-order model to simultaneously retrieve multiple vortical circulations.

The technique will be tested using various radar orientations (distance and angle) relative to the simulated tornado to determine the impact of less ideal radar-

vortex geometrical configurations. The low-order model and emulated radar beam will be extended to three dimensions to account for vertical shear and tilting of vortices with height. This will also allow for a larger range of elevation angles to be used in the analysis domain. Using a 3-D low-order model, however, will also increase the time required to run the retrieval in practice, and the complexity associated with the extra control parameters may also introduce additional local minima. The net advantage of extending the technique in this way is therefore unclear and will need to be investigated.

The technique will be tested against sets of real observations of tornadoes and their surrounding environments, including one or more datasets collected by a CASA radar testbed located in Oklahoma. Null cases will also be examined and objective detection criteria developed.

ACKNOWLEDGEMENTS

This work is supported in part by the Engineering Research Centers Program of the National Science Foundation under NSF award number 0313747.

REFERENCES

Gao, J.-D., M. Xue, A. Shapiro, and K. K. Droegemeier, 1999: A variational method for the analysis of three-dimensional wind fields from two Doppler radars. *Mon. Wea. Rev.*, **127**, 2128-2142.

Lee, W.-C., and F. D. Marks, 2000: Tropical cyclone kinematic structure retrieved from single Doppler radar observations. Part II: The GBVTD-simplex center finding algorithm. *Mon. Wea. Rev.,* **128**, 1925-1936.

——, W.-C., F. D. Marks, Jr., and R. E. Carbone, 1994: Velocity Track Display – A technique to extract real-time tropical cyclone circulations using a single airborne Doppler radar. *J. Atmos. Oceanic Technol.*, **11**, 337–356.

——, W.-C., J.-D. Jou, P.-L. Chang, and S.-M. Deng, 1999: Tropical cyclone kinematic structure retrieved from single Doppler radar observations. Part I: Interpretation of Doppler velocity patterns and the GBVTD technique. *Mon. Wea. Rev.,* **127**, 2419-2439.

Lhermitte, R. M., and D. Atlas, 1962: Precipitation motion by pulse Doppler. *Proc. Ninth Weather Radar Conf.*, Kansas City, MO, Amer. Meteor. Soc., 218-223.

McLaughlin, D., V. Chandrasekar, K. Droegemeier, S. Frasier, J. Kurose, F. Junyent, B. Philips, S. Cruz-Pol, and J. Colom, 2005: Distributed Collaborative Adaptive Sensing (DCAS) for improved detection, understanding, and predicting of atmospheric hazards. Preprints*, 85th AMS Annual Meeting,* San Diego, CA, Amer. Meteor. Soc.

Roux, F., and F. D. Marks, 1996: Extended velocity track display (EVTD): An improved processing method for Doppler radar observation of tropical cyclones. *J. Atmos. Oceanic Technol.*, **13**, 875–899.

Shapiro, A., J. J. Mewes, 1999: New formulations of Dual-Doppler wind analysis. *J. Atmos. Oceanic Technol.*, **16**, 782–792.

Waldteufel, P., and H. Corbin, 1979: On the analysis of single Doppler radar data. *J. Appl. Meteor.*, **18**, 532–542.

Xue, M., K. K. Droegemeier, V. Wong, A. Shapiro, K. Brewster, F. Carr,D. Weber, Y. Liu, and D. Wang, 2001: The Advanced Regional Prediction System (ARPS) – A multi-scale nonhydrostatic

atmospheric simulation and prediction tool. Part II: Model physics and applications. *Meteor. Atmos. Phys*., **76**, 143-165.